

Electronic structure of $\text{Cd}_{1-x}\text{Mn}_x\text{S}$ ternary semimagnetic alloys

A. Wall* and A. Franciosi

Department of Chemical Engineering and Materials Science, University of Minnesota, Minneapolis, Minnesota 55455

D. W. Niles

Department of Physics, University of Wisconsin, Madison, Wisconsin 53706

R. Reifenberger

Department of Physics, Purdue University, West Lafayette, Indiana 47907

C. Quaresima, M. Capozzi, and P. Perfetti

Istituto di Struttura della Materia, via Enrico Fermi 38, I-00044 Frascati, Italy

(Received 30 August 1989)

We present synchrotron-radiation photoemission studies of the electronic structure of $\text{Cd}_{1-x}\text{Mn}_x\text{S}$ alloys, together with results for the parent binary compound CdS. Analysis of the partial photoionization cross section at the Mn $3p$ - $3d$ resonance was conducted to investigate the Mn $3d$ contribution to the valence bands. We use $\text{Cd}_{1-x}\text{Mn}_x\text{S}$ as a test case to examine different methods of data reduction. A comparative analysis of constant-initial-state (CIS) spectra, ternary-binary difference curves, as well as resonance-antiresonance difference curves identifies a major Mn $3d$ density of states feature 3.12 ± 0.05 eV below the CdS valence-band maximum, together with relevant Mn $3d$ contribution to the electron states near the valence-band maximum and a broad satellite in the 4–8-eV range. A quantitative analysis of the Fano parameters derived from a least-squares fit of the CIS spectra allowed us to characterize the varying amount of Te p -Mn $3d$ hybridization in the valence states.

INTRODUCTION

Recent progress in our understanding of the properties of ternary semimagnetic semiconductors stems from the exploitation of synchrotron-radiation photoemission,^{1–8} extended x-ray-absorption fine structure (EXAFS),^{9–11} and inverse-photoemission spectroscopies:^{12,13} spectroscopies, together with the parallel development of realistic band-structure and total-energy calculations.^{14–20} All semimagnetic semiconductors studied to date are obtained by replacing cations in a II-VI compound semiconductor lattice with Mn or Fe atoms. Random ternary alloys of this kind are difficult to model theoretically, because of the double localized-itinerant nature of the $3d$ states, and because of the random nature of the alloy.

These ternary alloys have composition-dependent transport and optical properties, and also exhibit new magnetotransport and magneto-optical properties because of the spin-spin exchange interaction between band and impurity states.^{21–23} The resulting large g factors, giant magnetoresistance, and large values of the Faraday rotation could be exploited in optoelectronic devices. $\text{Cd}_{1-x}\text{Mn}_x\text{Te}$ alloys, for example, exhibit some of the

largest values of the Verdet coefficient encountered for wavelengths $< 1 \mu\text{m}$, and could be used to make efficient optical isolators.^{21–23}

Among the possible magnetic impurities that can be introduced in a II-VI compound semiconductor lattice, Mn plays a special role because of the $3d^5 4s^2$ configuration of the free atom. According to Hund's rule, the $3d^5$ electrons are expected to have parallel spins, and give rise to a relatively stable divalent configuration of the Mn atom. The divalent Mn atom can therefore easily replace cations in the II-VI lattice, and exhibits large solubility in most group-II selenides, tellurides, and sulfides. Crucial points which are still the subject of debate are the nature of the bonding of the magnetic impurity in the compound semiconductor matrix, localization and hybridization of the $3d$ orbitals and, in turn, the influence of the magnetic impurity on the stability of the host.²⁴

Photoemission spectroscopy is an ideal tool to investigate the electronic structure of these semiconductors, and we have recently presented systematic studies of $\text{Hg}_{1-x}\text{Mn}_x\text{Se}$,^{1–3} $\text{Cd}_{1-x}\text{Mn}_x\text{Se}$,² $\text{Zn}_{1-x}\text{Mn}_x\text{Se}$, $\text{Hg}_{1-x}\text{Mn}_x\text{Te}$,⁸ and $\text{Hg}_{1-x}\text{Fe}_x\text{Se}$ (Ref. 5) alloys. These results, together with those of Taniguchi *et al.*⁶ for

$\text{Cd}_{1-x}\text{Mn}_x\text{Te}$, and for the corresponding selenides and sulfides,⁷ isolated the $3d$ contribution to the electronic density of states (DOS) below E_F and pointed out, for example, a major Mn $3d$ feature 3.3–3.5 below the valence-band maximum (E_v) in all of these alloys. Some controversies still exist, though, in the detailed analysis of the photoemission results. Different authors employ different data reduction methods, and have at one time or another reported the existence of other Mn $3d$ DOS or shake-up features,^{7,25–27} or conflicted about the localization and hybridization of the Mn $3d$ states.^{7,8}

As far as the wide gap $\text{Cd}_{1-x}\text{Mn}_x\text{S}$ alloy is concerned, little information is available. We are aware of a single spectrum for an $x=0.3$ sample published in Ref. 7, which exhibits features qualitatively similar to those reported for $\text{Cd}_{1-x}\text{Mn}_x\text{Te}$ and $\text{Cd}_{1-x}\text{Mn}_x\text{Se}$. We are not aware of any detailed photon-energy-dependent studies of the photoemission cross section for $\text{Cd}_{1-x}\text{Mn}_x\text{S}$ in the literature. Here we expand the pioneering result of Ref. 7 and reexamine in detail the valence-band structure of $\text{Cd}_{1-x}\text{Mn}_x\text{S}$ discussing several analysis methods of the photoemission data.^{6–8} We show that the different methods yield consistent results, with a major Mn $3d$ contribution in $\text{Cd}_{1-x}\text{Mn}_x\text{S}$ emerging 3.12 ± 0.05 below the top of the CdS valence bands and substantial admixture of $3d$ character to the states near the leading edge of the valence band. We present a quantitative analysis of the valence cross section near the Mn $3p$ - $3d$ resonance, and discuss the experimental information *vis-à-vis* of the results for the selenide and telluride ternary series,^{1–8,11,21–27} drawing comparison with the trends of recent band-structure calculations.^{14–20}

EXPERIMENTAL PROCEDURE

Single crystals of $\text{Cd}_{1-x}\text{Mn}_x\text{S}$ with $x=0.10\pm 0.01$ were grown at Purdue University through a modified Bridgmann method. X-ray diffraction showed the sample to be single-phase single crystals. Single crystals of the binary parent compound CdS were obtained from a commercial source.

The experiments were performed at the synchrotron radiation facility ADONE (PULS) of the Italian National Laboratory of Frascati (Rome), with a Jobin-Yvon toroidal grating monochromator, in the photon energy range $30\leq h\nu\leq 80$ eV. Radiation from a high-intensity tungsten lamp was focused on the sample surface through a quartz viewport to eliminate charging. The samples were cleaved *in situ* in a photoelectron spectrometer (operating pressure less than 1×10^{-10} Torr) with variable degree of success at obtaining mirrorlike natural cleavage surfaces. The data discussed here are independent of cleave quality and provide information on the bulk electronic structure of these materials.

Angle-integrated photoelectron energy distribution curves (EDC's) were recorded with a commercial double-pass cylindrical mirror analyzer, and the overall resolution (electron plus photons) ranged from 0.25 to 0.7 eV in the $21\leq h\nu\leq 80$ eV photon energy range.

Constant-initial-state spectra were obtained by scanning under computer control the monochromator and the analyzer pass energy.^{28,29} The results of these studies are summarized in Figs. 1–6. The zero of the energy scale for the EDC's corresponds to the Fermi level E_F , as determined from the Fermi cutoff of a thick Au film deposited *a posteriori* onto the semiconductor surface.

RESULTS AND DISCUSSION

General valence-band features and valence-band maximum E_v

Valence-band EDC's for CdS and $\text{Cd}_{0.9}\text{Mn}_{0.1}\text{S}$ samples were recorded for $21 < h\nu < 80$ eV at 0.5 eV intervals in the photon energy range. Selected results are plotted in an expanded scale in Fig. 1. To facilitate a qualitative comparison of ternary and binary valence-band features for $\text{Cd}_{1-x}\text{Mn}_x\text{S}$ (solid line) and CdS (dashed line) the spectra have been normalized to the first major valence-band emission feature and are shown with binding energy referred to the position of the Fermi level E_F . Comparison with results for the binary II-VI compound semiconductor series³⁰ and DOS calculations for other ternary semimagnetic semiconductors^{14–18} allows us to identify for CdS in Fig. 1 a first DOS feature extending to about 5.0 eV below the Fermi level E_F as primarily S p derived. A second hybrid Cd s -S p DOS feature is visible at all photon energies for CdS at about 6.2 eV from E_F .

The Cd $4d$ core levels appear as a poorly resolved doublet in the leftmost section of Fig. 1, in a reduced scale ($\times 10$) relative to the valence-band features. The peak intensity of the overall $4d$ line (approximately correspondent to the bulk $4d_{5/2}$ contribution²⁸) was observed at 11.78 ± 0.08 eV and 11.82 ± 0.08 eV, respectively, in $\text{Cd}_{1-x}\text{Mn}_x\text{S}$ and CdS. The shoulder visible on the low binding-energy side of the Cd $4d$ line is likely to be due to emission from the S $3s$ levels, by analogy with the case of Te in $\text{Cd}_{1-x}\text{Mn}_x\text{Te}$ alloys.^{12,30–32} The normalization factor chosen in Fig. 1 yields a close match of the EDC's in correspondence of the background below the Cd $4d$ core features (14–15 eV below E_F) but gives Cd $4d$ integrated intensities³³ in $\text{Cd}_{1-x}\text{Mn}_x\text{S}$ relative to CdS systematically 10–15 % lower than those expected from the nominal sample stoichiometry. The most notable qualitative modifications of the valence-band emission induced by Mn in Fig. 1 are observed at photon energies at or above the Mn $3p$ - $3d$ resonance^{1–6} ($h\nu\sim 50$ eV). The ternary EDC's in this photon energy range show increased emission near the leading edge of the valence band, the emergence of a sharp emission feature at 5.33 ± 0.05 eV below E_F , and increased emission in the 6–10-eV binding energy range.

The existence of Mn-induced emission near the top of the valence band yields some complications in the determination of the position of the valence-band maximum E_v . The position of E_v is usually determined through a linear extrapolation of the leading edge of the valence

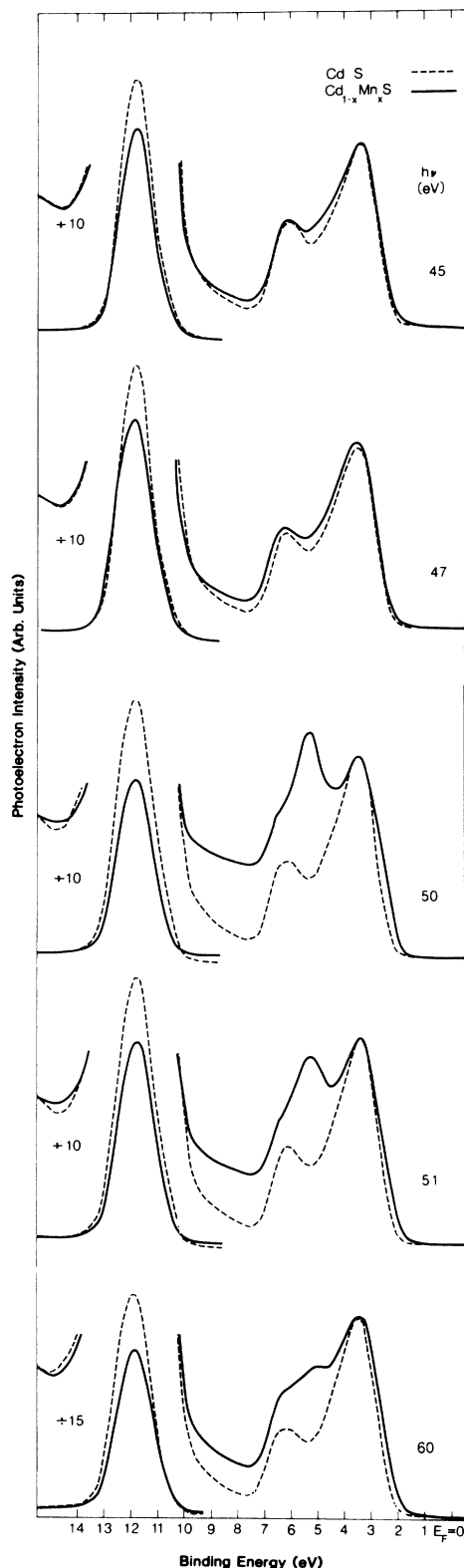


FIG. 1. Selected photoelectron energy distribution curves for the valence band and Cd 4d core emission from $\text{Cd}_{1-x}\text{Mn}_x\text{S}$ with $x=0.10$ (solid line) and CdS (dashed line). The spectra have been arbitrarily normalized and superimposed to emphasize line-shape changes. The binding energies are referred to the Fermi level E_F .

band, or through a least-squares fit of the valence-band edge to a suitably broadened theoretical density of states.³⁴ For semiconductors with reduced spin-orbit effects, such as CdS, both methods yield quantitatively consistent results.³² An application of the linear extrapolation method to the $\text{Cd}_{1-x}\text{Mn}_x\text{S}$ spectra in Fig. 1 would give a photon-energy-dependent position of E_v because of the variable Mn 3d contribution. We note, in particular, that at photon energies below the 3p-3d resonance, where the S p-state cross section dominates, E_v appears at 2.18 ± 0.08 eV in $\text{Cd}_{1-x}\text{Mn}_x\text{S}$ and 2.19 ± 0.07 eV in CdS, i.e., at the same position. At photon energies near the resonance ($h\nu=50$ eV), the corresponding values for E_v are, instead, 1.90 ± 0.08 eV ($\text{Cd}_{1-x}\text{Mn}_x\text{S}$) and 2.21 ± 0.08 eV (CdS). Above the resonance ($h\nu=60$ eV) the difference is somewhat reduced: $E_v=1.95 \pm 0.08$ eV ($\text{Cd}_{1-x}\text{Mn}_x\text{S}$) and 2.20 ± 0.08 eV (CdS).

In what follows, binding energies referred to E_v will be measured relative to the position of the valence-band maximum in CdS. This is justified in view of the fact that the linearly extrapolated value of E_v in the ternary is photon energy dependent and composition dependent, and in principle may not reflect an actual change in the one-electron density of states. Final-state effects may affect the photoemission-determined 3d contribution⁷ relative to the partial density of states because of the localized nature of the 3d states.^{16,17} The lack of any detectable shift of the Cd 4d core levels, as well as the Cd-S and S-p density of states features (at 6.25 and 3.5 eV, respectively, in Fig. 1) in going from the binary to the ternary alloy also suggests that the valence-band maximum of CdS is an appropriate reference level.

Mn 3d contribution

The characteristic Mn-3d photoionization cross section in the photon energy range of the Mn 3p \rightarrow 3d transition allows one to investigate the Mn 3d contribution to the valence bands.¹⁻⁸ The Mn 3d partial photoionization cross section exhibits a characteristic threefold enhancement at resonance in metallic and atomic Mn. This enhancement reflects the quantum-mechanical equivalence of different processes leading from the ground state to the same final state.¹² One process is the direct excitation

$$3p^6 3d^5 4(sp)^2 + h\nu \rightarrow 3p^6 3d^4 4(sp)^2 \epsilon f .$$

The other involves a 3p core excitation and a super Coster-Kronig decay:

$$3p^6 3d^5 4(sp)^2 h\nu \rightarrow 3p^5 3d^6 4(sp)^2 \rightarrow 3p^6 3d^4 (sp)^2 \epsilon f .$$

Two methods used to analyze the 3d contribution to the valence states involve ternary-binary valence EDC difference curves,²⁴ and resonance-antiresonance EDC difference curves.⁶ In Fig. 2 we show an example of the first method for $\text{Cd}_{0.90}\text{Mn}_{0.10}\text{S}$. Spectra for the ternary

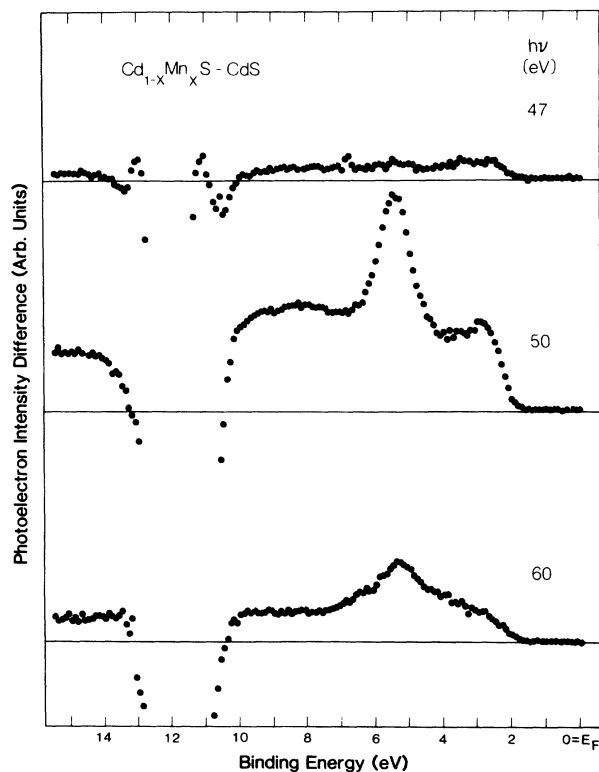


FIG. 2. Ternary-binary difference curves obtained from the EDC's in Fig. 1 after normalization of the EDC's to the integrated Cd $4d$ intensity scaled by the Cd concentration $(1-x)$. Photon energies of 47, 50, and 60 eV correspond, respectively, to antiresonance, resonance, and above-resonance conditions for the Mn $3p-3d$ photoexcitation cross section.

alloy and for CdS have been normalized to the integrated intensity of the Cd $4d$ cores scaled by a $(1-x)$ factor derived from x-ray microprobe analysis and subtracted from each other. The photon energies of 47, 50, and 60 eV selected in Fig. 2 approximately correspond, respectively, to antiresonance, resonance, and above-resonance conditions for the Mn $3d$ cross section.²⁴ The binding energies are referred to the Fermi level E_F , and the top of the CdS valence bands is at 2.20 ± 0.05 eV, as discussed in the previous section. The dip in the 10–13-eV range in Fig. 2 reflects the composition-dependent variation in the intensity of the Cd $4d$ emission going from the ternary alloy to the binary.

At antiresonance,²⁴ when the Mn $3d$ emission is suppressed (top section of Fig. 2) the ternary-binary difference curve is flat and relatively featureless in the 2–10-eV range. For photon energies at or above the Mn $3p-3d$ resonance, the increase in the Mn $3d$ photoionization cross section gives rise to a sharp dominant feature at 5.33 ± 0.05 eV (3.13 eV below the CdS valence-band maximum), to smaller and less structured features in the 2–4 and 6–10-eV binding energy ranges, and to an increased secondary electron background visible on both sides of the $4d$ -related dip (10–12 eV). The major Mn $3d$ emission feature in Fig. 2 is compellingly similar to those observed some 3.4–3.5 eV below the apparent valence-

band maximum in $\text{Hg}_{1-x}\text{Mn}_x\text{Se}$,^{1,2} $\text{Cd}_{1-x}\text{Mn}_x\text{Se}$,^{2,3} $\text{Zn}_{1-x}\text{Mn}_x\text{Se}$,² $\text{Hg}_{1-x}\text{Mn}_x\text{Te}$,⁴ and $\text{Cd}_{1-x}\text{Mn}_x\text{Te}$.^{8,24}

The method employed in Refs. 1–4 to calculate ternary-binary difference curves differs from that employed here in two respects: first, the subtraction of a computer-fitted polynomial secondary background in Refs. 1–4 tends to deemphasize the broad emission feature observed in Fig. 2 in the 8–10-eV region; secondly, the normalization to the apparent main anion p DOS feature used in Refs. 1–4 would yield ternary versus binary EDC amplitudes similar to those observed in Fig. 1. A ternary-binary difference curve calculated with such a normalization would underestimate the Mn contribution. In combination with the background subtraction procedure, this tends to increase the importance of the main Mn feature relative to the broad low- and high-energy structure.

In Refs. 1–5 we interpreted the main Mn-derived feature as primarily $3d$ derived, with little or no evidence of hybridization with anion p states. This interpretation was proposed on the basis of an analysis of the resonant behavior, but came recently under some criticism.⁷ Taniguchi *et al.*^{6,7} presented a different data reduction of resonant photoemission data (resonance-antiresonance difference curves) for several ternary semimagnetic semiconductors, together with semiempirical calculations of the final state of the Mn $3d$ photoemission process in MnTe_4^{6-} clusters. They concluded that the main Mn $3d$ feature mostly corresponds to a $d^5\bar{L}$ final state where the $3d$ hole is screened through charge transfer from a Te $5p$ -derived ligand orbital \bar{L} .

Although in the framework of the configuration interaction cluster model employed⁷ $d-p$ hybridization cannot be incorporated in the ground state, the authors of Ref. 7 considered it included in the final state as a mixing between the d^4 (unscreened) and $d^5\bar{L}$ (ligand-screened) configurations. Within the limits of this assumption, the main Mn $3d$ feature should exhibit substantial $p-d$ hybridization. The apparent controversy in the interpretation of the resonant photoemission results of Refs. 1–8 stimulated our interest in considering all of the proposed methods of data reduction in the case of $\text{Cd}_{1-x}\text{Mn}_x\text{S}$.

In Fig. 3 we show examples of resonance-antiresonance difference curves for $\text{Cd}_{0.90}\text{Mn}_{0.10}\text{S}$. The method employed is the same proposed in Ref. 6. EDC's for the ternary semiconductor at photon energies near resonance and antiresonance are normalized to the Cd $4d$ integrated intensity, and difference curves are then calculated to emphasize the Mn $3d$ character. In Fig. 3 we plot such difference curves for several choices of photon energies $h\nu_R$ near resonance and $h\nu_{AR}$ near antiresonance. We also present (marked by an asterisk) a result for a different cleave of poor quality to illustrate the range of cleave dependence observed in the results. Comparison of Figs. 2 and 3 should test our identifications.

The topmost spectrum in Fig. 3 was obtained with $h\nu_{AR}=47$ eV, and can be directly compared with the one reported by Taniguchi *et al.* in Ref. 7 ($h\nu_R=49.5$ eV, $h\nu_{AR}=47$ eV). The agreement is good, although we did not subtract the secondary background in order to avoid arbitrary variations in the relative amplitude of the

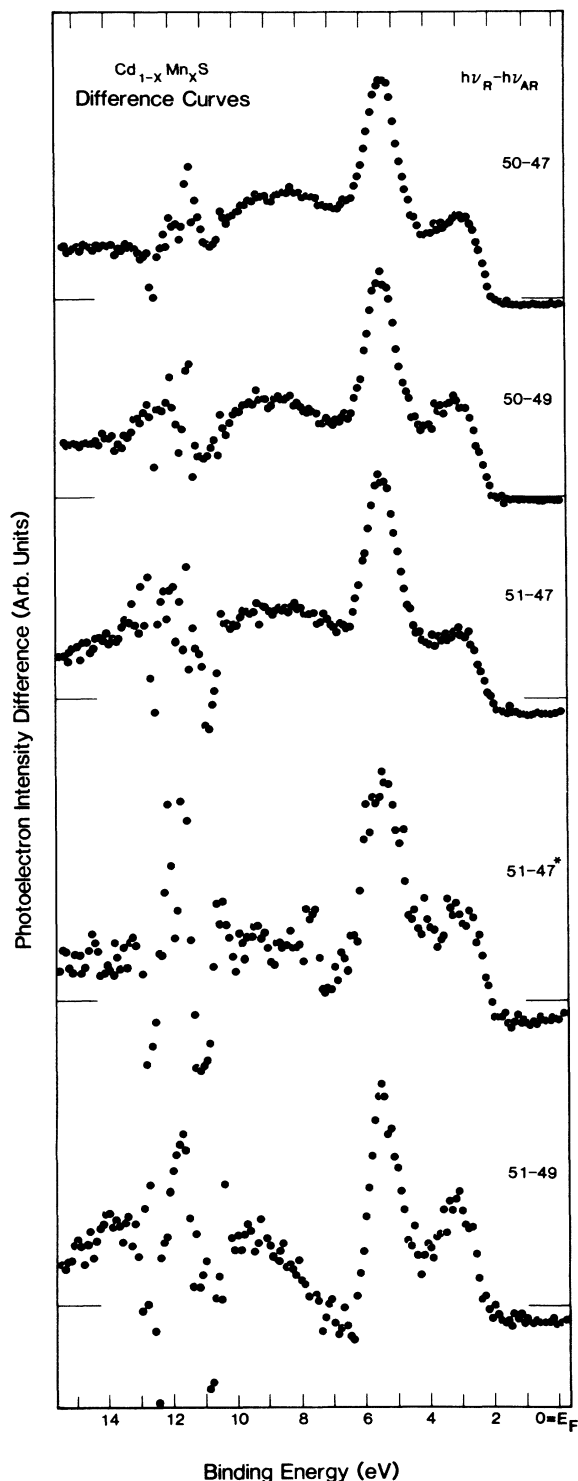


FIG. 3 Resonance-antiresonance difference curves obtained from $\text{Cd}_{1-x}\text{Mn}_x\text{S}$ for different choices of photon energies near resonance ($h\nu_R$) and antiresonance ($h\nu_{AR}$). The difference curves have been obtained from valence-band EDC's after normalization to the integrated intensity of the Cd 4d core levels, and emphasize the Mn 3d contribution to the valence-band emission. The spectrum marked by an asterisk illustrates the dependence of the spectra features on cleave quality.

different spectral features. The cross sections of the 5s, 3p, and 4d states also vary with photon energy, so that difference curves of this kind may introduce features that do not reflect the 3d contribution. The normalization to the integrated intensity of the Cd 4d feature is therefore artificial, and is introduced only to eliminate some of the spurious features that appear in the difference curves. The experimental energy resolution and the secondary background also vary with photon energy. In principle, the smallest possible $h\nu_R - h\nu_{AR}$ window should be employed in order to minimize the cross-section variation of the non-3d features. To reduce some of the ambiguities, one should look for common features with are independent of the choice of the photon energies and cleave quality.

Of the spectral features identified in Fig. 3, two appear unambiguously in all of the difference curves, namely the dominant Mn-derived feature at 5.35 eV and the low binding-energy feature due to the modification of the leading edge of the valence band. The broad satellite in the 6–10 eV range also appears in several, but not all, of the difference curves in Fig. 3, pointing out differences in the photoionization cross section of the corresponding states relative to the main Mn 3d spectral contribution. In extracting systematic trends⁷ for the Mn 3d contribution in different ternary semimagnetic samples, one should consider that the relative amplitude of the different 3d features is somewhat dependent on the choice of the $h\nu_R - h\nu_{AR}$ window and on the estimate of the secondary background contribution.

In Fig. 4 we compare selected ternary-binary difference curves (solid circles, $h\nu = 51$ eV in the topmost section, $h\nu = 50$ eV in the bottom-most section) with selected resonance-antiresonance difference curves from Fig. 3 (solid squares and open triangles) for four different choices of the $h\nu_R - h\nu_{AR}$ window. Although the relative intensity of the different Mn 3d features in Fig. 4 does not remain constant in the series, the general qualitative agreement is remarkable. The actual interpretation of the different Mn 3d features in terms of one-electron DOS features and/or final-state effects can be provided only through comparison with theory and through a detailed quantitative analysis of the photoionization cross section.

We are not aware of any published band-structure calculation for $\text{Cd}_{1-x}\text{Mn}_x\text{S}$. However, calculations for $\text{Cd}_{1-x}\text{Mn}_x\text{Te}$ have been performed by a number of authors^{14–17,19,20} and there are strong similarities in the Mn 3d signature if one compares ternary semimagnetic sulfides, selenides, and tellurides.^{1–8,12,24} Calculations for MnTe by means of a spin-unrestricted localized pseudofunction method in the local density approximation¹² are also in striking agreement with photoemission experiments for $\text{Cd}_{1-x}\text{Mn}_x\text{Te}$. Such calculations showed¹² that the Mn electronic configuration is $(d\uparrow)^5(s\uparrow)(p\uparrow)$, rather than $(d\uparrow)^5s^2$ in these materials, and allowed an explanation of the anomalous Curie temperatures of these alloys.¹⁸ The implication is that the Mn 3d spectral contribution mostly reflects the local Mn-anion coordination, and is surprisingly well described by the one-electron calculation, except for a broad satellite in the 6–9-eV energy

range below E_v .

Taking into account an experimental broadening of 0.3 eV, the calculation predicts¹² a main $3d$ spectral feature 3.5 eV below the top of the linearly extrapolated position of E_v in the ternary, with a full width at half maximum of 1.3 eV. Only the high binding-energy portion of such features exhibits some superposition with Te-derived states. Other smaller Mn $3d$ features at 0.8 and 1.6

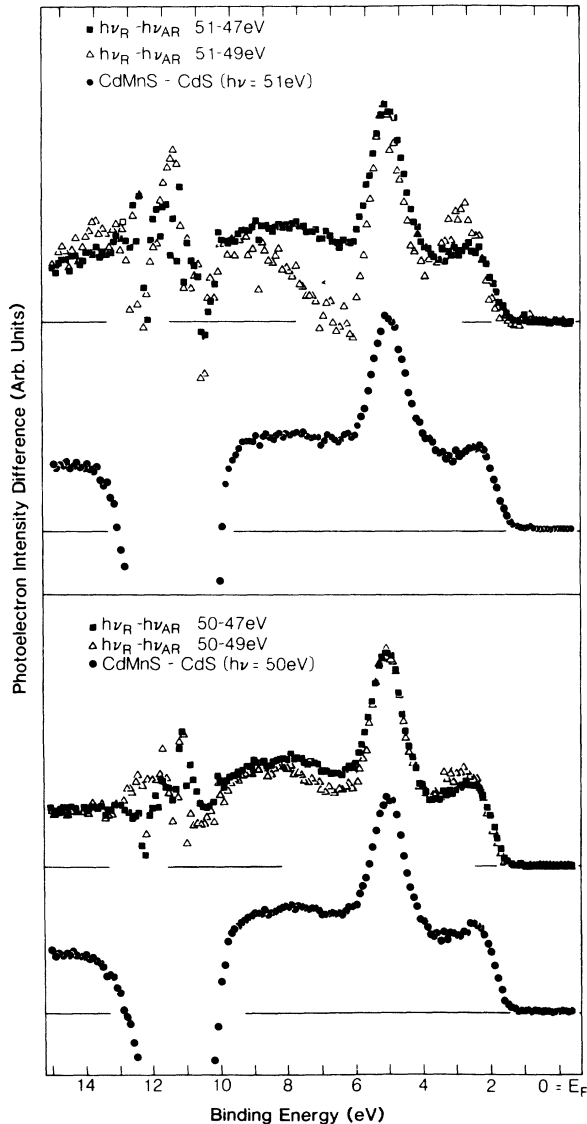


FIG. 4. Comparison of ternary-binary difference curve with resonance-antiresonance difference curves for $\text{Cd}_{0.90}\text{Mn}_{0.10}\text{S}$. Top, solid circles: ternary-binary difference curve at $h\nu=51$ eV. Top, open triangles: resonance (R) -antiresonance (AR) difference curve for $h\nu_R=51$ eV and $h\nu_{AR}=49$ eV. Top, solid squares: resonance-antiresonance difference curve for $h\nu_R=51$ eV and $h\nu_{AR}=47$ eV. Bottom, solid circles: ternary-binary difference curve at $h\nu=50$ eV. Bottom, open triangles: resonance-antiresonance difference curve for $h\nu_R=50$ eV and $h\nu_{AR}=47$ eV.

should exhibit, instead, substantial hybridization with anion p states. If we refer the theoretical predictions to the binding-energy scale used in this work, we would expect $3d$ structure 0.5, 1.3, and 3.2 eV below the CdS valence-band maximum, i.e., at 2.7, 3.5, and 5.4 eV relative to E_F in Fig. 4. Experimentally we do observe structure at 2.6 and 5.35 eV in Fig. 4, and structure at 3.5 eV may be observed at least in some of the ternary-binary difference curves. Such a good agreement is somewhat surprising, since the calculation was performed for the telluride rather than the sulfide. From the calculation we would expect a much larger d - p hybridization for the valence-band feature in the 2–4-eV energy range than for the main $3d$ feature at 5.35 eV.

The semiempirical cluster calculation by Fujimori and co-workers⁷ also obtains good agreement with experiment. In the configuration interaction picture, a number of multiplet lines deriving from d^4 and $d^5\bar{L}$ final-state components correspond to an unscreened $3d$ hole (d^4), or to a $3d$ hole screened by charge transfer ($d^5\bar{L}$) from a Te $5p$ -derived ligand orbital \bar{L} (π or σ) to a d orbital (e_g or t_{2g}). In Ref. 7 the authors include lifetime and experimental broadening to yield perfect agreement with the experimental resonance-antiresonance difference curves. Unfortunately, such an agreement may be fortuitous, since the energy differences between the final-state configurations and the lifetime of each final-state configuration are not known *a priori*. The method contains, therefore, eight adjustable parameters, resulting in a basic line shape involving three spectral features of arbitrary separation and arbitrary relative intensity. In these conditions the theoretical curve can reproduce almost any experimental line shape. Therefore we have to emphasize that the validity of this method can be judged only from the accuracy of its predictions about the character and hybridization of the different experimental features. This will be the topic of the next section.

The cluster model⁷ does account for the broad satellite that does not appear in any one-electron calculation.^{12–20} We note that a broad emission feature some 6.8 eV below the apparent position of E_v in $\text{Cd}_{1-x}\text{Mn}_x\text{Te}$ was first reported by Orłowski²⁵ and later assigned by Webb *et al.*²⁶ to a shake-up satellite of the main $3d$ feature. Similar broad features have been observed in the same energy range in MnO and NiO,^{35,36} and assigned in both cases to multielectron satellites. In the model by Fujimori and co-workers,⁷ the satellite is mostly due to the unscreened d^4 final state, and should therefore exhibit a relatively pure Mn $3d$ character with no evidence of d - p hybridization. In a recent inverse photoemission study of $\text{Cd}_{1-x}\text{Mn}_x\text{Te}$,^{12,13} we found a value of 8.32 ± 0.4 eV for the $d\uparrow$ - $d\downarrow$ exchange splitting, comparable with the values assumed for Mott insulators such as MnO (9 eV). We proposed that the similar energy position of the 6–9-eV satellite in $\text{Cd}_{1-x}\text{Mn}_x\text{Te}$ and MnO is a reflection of the similar $3d$ correlation energy in these materials. If this interpretation is correct, since in $\text{Cd}_{1-x}\text{Mn}_x\text{S}$ (Fig. 4) the satellite roughly appears in the same energy range as in $\text{Cd}_{1-x}\text{Mn}_x\text{Te}$, the implication would be that the Mn $3d$ correlation energy does not vary substantially in going from $\text{Cd}_{1-x}\text{Mn}_x\text{Te}$ to $\text{Cd}_{1-x}\text{Mn}_x\text{S}$.

Photoionization cross section and d - p hybridization

We used constant-initial-state (CIS) photoemission spectra^{28,29} from CdS and $\text{Cd}_{0.90}\text{Mn}_{0.10}\text{S}$ samples for different initial-state energies within the valence bands, to examine the origin of the $3d$ -related structure near the top of the valence bands (2–4 eV in Fig. 4), the dominant feature at 5.35 eV, and the broad satellite in the 6–10-eV range. The resonant behavior of the Mn $3d$ states³⁷ can be analyzed through a formalism introduced by Fano³⁸ and later extended to the transition metals by Davis and Feldkamp³⁹ and Yafet.⁴⁰ At the $3p$ - $3d$ resonance the interference of a discrete excited state with the continuum yields a photon-energy-dependent $3d$ absorption line shape (Fano line shape) that can be expressed as^{37,38}

$$I(\nu) = \frac{(q + \varepsilon)^2}{1 + \varepsilon^2}$$

with

$$\varepsilon = (h\nu - E_0) / \Gamma,$$

where ε is a reduced energy parameter, q an asymmetry parameter, and the parameters E_0 and Γ determine, respectively, the center and the width of the resonant line.³⁹ The parameter E_0 is equal to the energy of the discrete state in the absence of interference minus a Coulomb-dependent energy shift $|F|$. F represents the shift of the resonance energy due to the interaction with the continuum,³⁷ and depends on Auger matrix elements between the discrete $3p^5 3d^6 4(sp)^2$ excited state of Mn and the $3p^6 d^4 (sp)^j \varepsilon l$ ($i + j = 6$) states of the continuum. The parameter Γ depends on the same integrals, but increases with decreasing F (or increasing $|F|$).³⁷

The asymmetry parameter q depends on the dipole transition probabilities from the ground state to the continuum states, and to the discrete excited states modified by the Coulomb interaction with the continuum. It is also affected directly by Auger matrix elements between continuum and discrete states.³⁷ The main contribution to the resonant line shape involves transitions to the 6P configuration at $h\nu \sim 50$ eV.^{7,8,39}

Representative CIS ratios for $\text{Cd}_{1-x}\text{Mn}_x\text{S}$ at different initial-state energies are shown in Figs. 5 and 6 together with the result of least-squares fit of the experimental data to the theoretical $I(\nu)$ line shape. The experimental spectra (solid circles) were obtained by measuring CIS spectra at a given initial energy for the ternary and for the binary semiconductor, and calculating the *ratio* of the two to eliminate the dependence on monochromator throughput and reduce the contribution of the binary semiconductor cross section.^{41,42}

We examined different choices of the energy “window” in which the theoretical $I(\nu)$ curve was fitted to the experimental data, and the effect of window size on q , Γ , and E_0 . This was necessary, since in principle such parameters are photon energy dependent.^{38–40} Davis and Feldkamp³⁹ have shown that a resonant line shape that employs constant values for q , Γ , and E_0 (evaluated at resonance, $h\nu \sim 50$ eV) will reproduce the true energy dependence of the cross section within a relatively narrow energy window ($47 < h\nu < 53$ eV) about E_0 . Further-

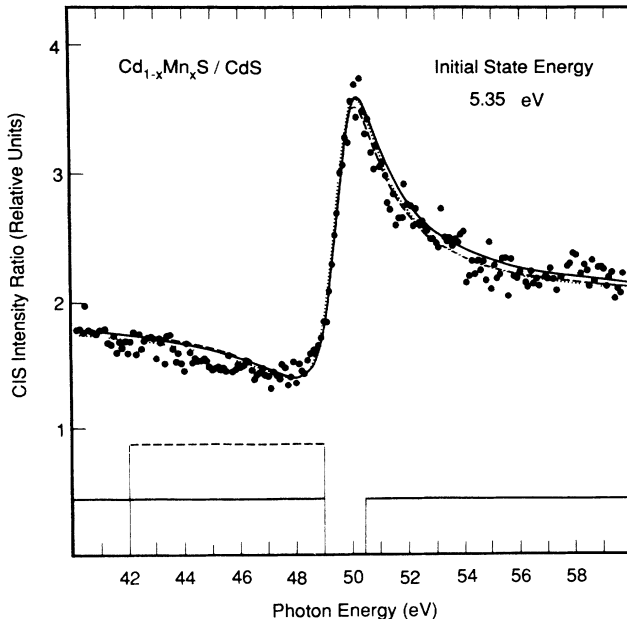


FIG. 5. Relative photoionization cross section (solid circles) of valence states 5.35 eV below E_F in $\text{Cd}_{1-x}\text{Mn}_x\text{Se}$ vs CdS, from the ratio of the corresponding constant-initial-state (CIS) spectra (Ref. 42). Solid line: result of at least-squares fit of the experimental point in terms of a Fano line shape in an energy window $49 < h\nu < 50.4$ eV. Dashed line: result of a fit in a $40 < h\nu < 42$ and $49 < h\nu < 60$ eV energy window. Dotted line: result of a fit in a $40 < h\nu < 60$ -eV photon energy window. The photon energy windows used for each fit are schematically illustrated in the bottom-most section of the figure.

more, other Mn-related transitions may produce additional spectral features superimposed to the main 6P resonance, making the determination of Γ , E_0 , and q less reliable. For example, absorption measurements in Mn vapor indicate that weaker transitions to 6D and 6F states may obscure the 6P antiresonance.^{39,43}

In order to eliminate possible spurious contributions and obtain the best possible estimates of q , Γ , and E_0 , it is therefore advisable to restrict the least-squares fitting to a relatively narrow energy range about E_0 . That this is indeed possible is illustrated in Fig. 5, where we compare the CIS ratio for an initial-state energy of 5.35 eV (corresponding to the major $3d$ emission feature) with three theoretical $I(\nu)$ line shapes (solid, dashed, and dotted lines) corresponding to the three fitting energy windows indicated in the bottom-most section of the figure (solid line CIS, $49 < h\nu < 50.4$ eV; dashed line CIS, $40 < h\nu < 42$ and $49 < h\nu < 60$ eV; dotted line CIS, $40 < h\nu < 60$ eV). Figure 5 demonstrates that we can use a narrow energy window about E_0 to obtain a satisfactory fit of the overall Fano line.

To obtain reliable parameters we considered several narrow energy windows in the $49 < h\nu < 53$ – 58 -eV range, obtained a best fit for each window, and took average values of q , Γ , and E_0 . As experimental uncertainty on the fitting parameters we took the maximum variation of the parameters with window size. The results are illus-

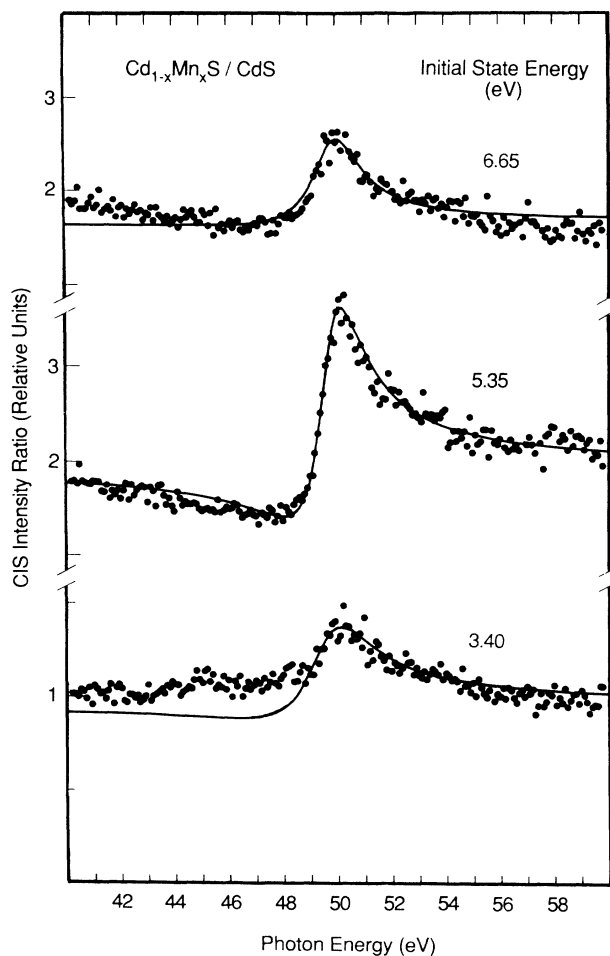


FIG. 6. CIS ratios for the different $3d$ features identified in Figs. 2–4. These partial cross sections were fitted to a theoretical Fano line shape (solid line) in a narrow energy window about the center of the line. The resulting fitting parameters are given in Table I. Top: CIS ratio for initial states at 3.4 eV, representative of the Mn $3d$ emission within 2 eV from the top of the valence bands. Middle: CIS ratio for initial states at 5.35 eV, corresponding to the major Mn $3d$ emission feature in Figs. 1–4. Bottom: CIS ratio for initial-state energy of 6.65 eV, corresponding to the broad satellite of the main $3d$ line in Figs. 2–4.

trated in Fig. 6 for initial-state energies of 3.4, 5.35, and 6.65 eV, corresponding to the three characteristic Mn $3d$ emission features identified in the previous section. The numerical values of the fitting parameters⁴⁴ are listed in Table I.

The CIS ratio in Fig. 5 and in the midsection of Fig. 6

corresponds to the major Mn $3d$ feature 5.35 eV below E_F and shows the strongest resonant enhancement. The approximately threefold (2.8) increase in the photoemission cross section at resonance is similar to that observed in the optical-absorption coefficient of metallic Mn.³⁷ The CIS ratio displays an unambiguous Fano line shape with little uncertainty in the values of the fitting parameters (Table I). The asymmetry parameter $q = 1.75 \pm 0.05$ appears smaller than that observed in the optical-absorption coefficient of metallic Mn (2.0 ± 0.10 eV).^{37,39} The relatively small value of q may be explained by an effect predicted by Yafet,⁴⁰ who considered the differences between photoemission and purely optical-absorption resonances. He concluded⁴⁰ that while Γ and E_0 should remain the same, the value of q may be reduced in photoemission of an amount dependent upon the strength of the Auger transition probability. Such a behavior has been verified experimentally in the case of metallic Ni.^{40,45}

In previous work on ternary semimagnetic selenides and tellurides²⁴ we have argued that the strength of the resonance enhancement is related to the overlap of the p core hole with the d valence states, and that if the d states become hybridized the overlap should be reduced and the enhancement diminished. Correspondingly, some resonance enhancement should appear in the cross section of the extra atomic states that gained d character through hybridization. This phenomenon has been observed in resonant photoemission studies of $3d$, $4d$, and $4f$ compounds,^{46,47} and can be used in the case of ternary semimagnetic semiconductor to investigate $3d$ hybridization with anion p states.

The CIS ratio in the topmost section of Fig. 6 indicates that the strength of the resonance for states within 2 eV from E_v is relatively small, with a 40% increase in intensity from antiresonance to resonance. The asymmetry parameter q is strongly dependent on the size of the energy window used for the fit, and carries a substantial uncertainty (2.25 ± 0.50). More insight is provided by the values of Γ (1.40 ± 0.15 eV) and E_0 (49.55 ± 0.15 eV) in Table I. The increase in width Γ and the shift observed for E_0 relative to values obtained for the major Mn 5.35 V feature are consistent with an increase in the width of the excited state.^{39,40} We suggest that hybridization of the $3d$ orbitals with S $3p$ orbitals may cause an increase in the width of the $3d$ states relative to the atomic case, and explain the behavior of Γ and F . Therefore, the reduced resonant enhancement and the trend of Γ and E_0 would all support the presence of high p - d hybridization for Mn states within 2 eV of E_v , as compared with states near

TABLE I. Fano parameters obtained from a least-squares fit of the experimental CIS ratios in Fig. 6 (initial state energies E_i of 3.4, 5.35, and 6.65 eV) in terms of Fano line shapes. Column 1: asymmetry parameter q . Column 2: energy width Γ of the resonance line, in eV. Column 3: center of the resonance line E_0 , in eV.

	q	Γ (eV)	E_0 (eV)
CIS ($E_i = 3.4$ eV)	2.25 ± 0.50	1.40 ± 0.15	49.55 ± 0.15
CIS ($E_i = 5.35$ eV)	1.75 ± 0.05	0.92 ± 0.03	49.73 ± 0.03
CIS ($E_i = 6.65$ eV)	< 3.25	1.05 ± 0.15	49.90 ± 0.15

3.13 eV, in agreement with the trends observed in one-electron band calculations.^{12-18,44} We note that in the configuration-interaction cluster calculations⁷ both sets of states are mostly due to the $d^5\bar{L}$ configuration, and should therefore exhibit a similar degree of p - d hybridization.

The CIS ratio in the bottom-most section of Fig. 6 corresponds to an initial energy of 6.65 eV, and is representative of the relative cross section of the broad 6-10 satellite in Figs. 2-4. The line shape appears qualitatively different from that observed in the middle and topmost sections of Fig. 6, with an increased asymmetry, evidence of nonresonant contributions in the 43-48-eV photon energy range, and a reduced resonant enhancement. The results of our fitting procedure in Table I show little uncertainty in Γ and E_0 , while the value of q carries a large uncertainty, since the Fano line shape is quite insensitive to variations of q when $q > 3$. The values of Γ and E_0 remain consistent with those observed for the main $3d$ emission at 5.33 eV, while the value of q is at least 80% higher than in the previous case. In the case of the 6 eV $3d$ satellite in Ni,⁴⁵ Davis and Feldkamp³⁹ have shown that the electron-electron interaction may modify the Auger intensity in the region of the satellite and give rise to an increase in the q factor relative to the resonance of the main $3d$ line. We conclude that the similarity of Γ and E_0 for states at 6.65 and 5.35 eV and the increase in q support the proposed $3d$ -related many-electron origin of the 6-10-eV structure.⁷

CONCLUSIONS

We have examined several methods of analysis of the Mn $3d$ contribution to the valence states of $\text{Cd}_{1-x}\text{Mn}_x\text{S}$ with consistent results. A detailed comparison of the relative cross section of the valence states in $\text{Cd}_{1-x}\text{Mn}_x\text{S}$ and CdS, and the results of one-electron calculations of the electronic structure for related systems, indicate that $3d$ states within 2 eV from the valence-band maximum exhibit the highest degree of hybridization with S p

states. The major $3d$ emission feature observed 3.13 eV below the top of the CdS valence bands exhibits comparatively low hybridization. First-principles one-electron calculations for MnTe show a surprising degree of agreement with experimental $\text{Cd}_{1-x}\text{Mn}_x\text{S}$ resonance spectra, and can reproduce the major Mn $3d$ features of the ternary semimagnetic semiconductor without postulating major final-state effects. However, only the semiempirical cluster of Fujimori and co-workers can account for the existence of the satellite.

We believe that in the near future much will be learned from a careful consideration of the photoionization cross section of the valence states in narrow-gap versus wide-gap ternary semimagnetic semiconductors. The systematic variation in the relative intensity of the different $3d$ features from compound to compound should clarify the importance of $d^5\bar{L}$ final-state charge transfer, d - p initial-state hybridization, and screening by conduction electrons in determining the experimental $3d$ contribution to the electronic structure, and the validity of the one-electron approximation.

ACKNOWLEDGMENTS

This work was supported, in part by Office of Naval Research (ONR) of the U.S. Department of Defense and by the Center for Interfacial Engineering at the University of Minnesota. The crystal growth at Purdue University was supported by the National Science Foundation (NSF). One of us (D.N.) would like to acknowledge the support of the NSF through Grant No. DMR-82-00518. We thank J. K. Furdyna for providing us with the samples used in the present studies and for encouragement and support, L. C. Davis, J. D. Dow, L. Ley, and M. Taniguchi for useful discussions. We are also grateful for the microprobe analysis by D. Yoder-Short and F. Pool. We are in debt to a number of colleagues who provided us with results of their work prior to publication: C. Balzarotti, M. De Crescenzi, H. Ehrenreich, O. Gunnarsson, K. Haas, A. Ramdas, and A. Zunger.

*Present address: IBM Corporation, Rochester, MN 55901.

¹A. Franciosi, C. Caprile, and R. Reifenberger, *Phys. Rev. B* **31**, 8061 (1985); A. Franciosi, R. Reifenberger, and J. K. Furdyna, *J. Vac. Sci. Technol. A* **3**, 124 (1985).

²A. Franciosi, S. Chang, C. Caprile, R. Reifenberger, and U. Debska, *J. Vac. Sci. Technol. A* **3**, 926 (1985).

³A. Franciosi, S. Chang, R. Reifenberger, U. Debska, and R. Riedel, *Phys. Rev. B* **32**, 6682 (1985).

⁴A. Wall, C. Caprile, A. Franciosi, M. Vaziri, and R. Reifenberger, *J. Vac. Sci. Technol. A* **4**, 818 (1986).

⁵A. Wall, C. Caprile, A. Franciosi, R. Reifenberger, U. Debska, and J. K. Furdyna, *J. Vac. Sci. Technol. A* **4**, 2010 (1986).

⁶M. Taniguchi, L. Ley, R. L. Johnson, J. Ghijsen, and M. Cardona, *Phys. Rev. B* **33**, 1206 (1986); L. Ley, M. Taniguchi, J. Ghijsen, R. L. Johnson, and A. Fujimori, *ibid.* **35**, 2839 (1987).

⁷M. Taniguchi, M. Fujimori, M. Fujisawa, T. Mori, I. Souma, and Y. Oka, *Solid State Commun.* **62**, 431 (1987).

⁸A. Wall, S. Chang, P. Philip, C. Caprile, A. Franciosi, R. Reifenberger, and F. Pool, *J. Vac. Sci. Technol. A* **5**, 2051 (1987), and references therein.

⁹A. Balzarotti, A. Kisiel, N. Motta, M. Zimnal-Starnawska, M. T. Czyzyk, and M. Podgorny, *Prog. Cryst. Growth Charact.* **10**, 55 (1985).

¹⁰A. Balzarotti, M. Czyzyk, A. Kisiel, N. Motta, M. Podgorny, and M. T. Zimnal-Starnawska, *Phys. Rev. B* **30**, 2295 (1985).

¹¹A. Balzarotti, M. Czyzyk, A. Kisiel, N. Motta, M. Podgorny, and M. T. Zimnal-Starnawska, *Phys. Rev. B* **30**, 7526 (1985).

¹²A. Franciosi, A. Wall, Y. Gao, J. H. Weaver, M.-H. Tsai, J. D. Dow, R. V. Kasowski, R. Reifenberger, and F. Pool, *Phys. Rev. B* **40**, 12009 (1989).

¹³A. Franciosi, A. Wall, Y. Gao, J. H. Weaver, S. Chang, A. Raisanen, and B. Rehil, in *Proceedings of the 19th International Conference on the Physics of Semiconductors*, edited by W. Zawadzki (IOP, Polish Academy of Sciences, Warsaw, 1988), p. 1263.

- ¹⁴B. E. Larson, K. C. Hass, H. Ehrenreich, and A. E. Carlsson, *Solid State Commun.* **56**, 347 (1985).
- ¹⁵H. Ehrenreich, K. C. Hass, N. F. Johnson, B. E. Larson, and R. J. Lampert, in *Proceedings of the 18th International Conference on the Physics of Semiconductors*, edited by O. Engstrom (World Scientific, Singapore, 1987), p. 1751; K. Hass (private communication).
- ¹⁶S.-H. Wei and A. Zunger, *Phys. Rev. B* **35**, 2340 (1987).
- ¹⁷S.-H. Wei and Z. Zunger, *Phys. Rev. Lett.* **56**, 2391 (1986).
- ¹⁸M.-H. Tsai, J. D. Dow, R. V. Kasowski, A. Wall, and A. Franciosi, *Solid State Commun.* **69**, 1131 (1989).
- ¹⁹M. Podgorny, *Z. Phys. B* **69**, 501 (1988).
- ²⁰J. Masek, B. Velicky, and V. Janis, *Acta Physica Polonica A* **69**, 1107 (1986).
- ²¹J. K. Furdyna, *J. Appl. Phys.* **53**, 7637 (1982).
- ²²N. B. Brandt and V. V. Moshchalkov, *J. Appl. Phys.* **53**, 7637 (1984).
- ²³R. R. Galazka and J. Kossut, *Narrow Gap Semiconductors: Physics and Applications*, Vol. 133 of *Lecture Notes in Physics Series* (Springer, Berlin, 1980).
- ²⁴A. Franciosi, in *Diluted Magnetic (Semimagnetic) Semiconductors*, edited by R. L. Aggarwal, J. K. Furdyna, and S. von Molnar (Materials Research Society, Pittsburgh, 1987), p. 175, and references therein.
- ²⁵B. A. Orlovski, *Phys. Status Solidi B* **95**, K31 (1979).
- ²⁶C. Webb, M. Kaminska, M. Lichtensteiger, and J. Lagowski, *Solid State Commun.* **40**, 609 (1981).
- ²⁷P. Oelhafen, M. P. Vecchi, J. L. Freeouf, and V. L. Moruzzi, *Solid State Commun.* **50**, 749 (1984).
- ²⁸See, for example, G. Margaritondo and A. Franciosi, *Ann. Rev. Mater. Sci.* **14**, 67 (1984), and references therein.
- ²⁹G. Margaritondo and J. H. Weaver, in *Methods of Experimental Physics: Surfaces*, edited by M. G. Lagally and R. L. Park (Academic, New York, 1983).
- ³⁰N. J. Shevchik, J. Tejada, M. Cardona, and D. W. Langer, *Phys. Status Solidi B* **59**, 87 (1973).
- ³¹The Cd 4d line shape in II-VI compound semiconductors contains a bulk and a surface-shifted contribution: see P. John, T. Miller, T. C. Hsieh, A. P. Shapiro, A. L. Wach, and T.-C. Chiang, *Phys. Rev. B* **34** 6704 (1986), and K. C. Prince, G. Paolucci, V. Chab, M. Surman, and A. M. Bradshaw, *Surf. Sci.* **206**, L871 (1988) for results for CdTe.
- ³²A. Wall, A. Franciosi, Y. Gao, J. H. Weaver, and J. R. Chelikowsky, unpublished.
- ³³Integrated core photoemission intensities after subtraction of a polynomial secondary-electron background.
- ³⁴E. A. Kraut, R. W. Grant, J. R. Waldrop, and S. P. Kowalczyk, *Phys. Rev. B* **28**, 1965 (1983).
- ³⁵D. E. Eastman and J. L. Freeouf, *Phys. Rev. Lett.* **34**, 395 (1975).
- ³⁶G. K. Wertheim and S. Hüfner, *Phys. Rev. Lett.* **28**, 1028 (1972).
- ³⁷B. Sonntag, R. Haensel, and C. Kunz, *Solid State Commun.* **7**, 597 (1969).
- ³⁸U. Fano, *Phys. Rev.* **124**, 1866 (1961).
- ³⁹L. C. Davis and L. A. Feldkamp, *Phys. Rev. B* **23**, 6239 (1981); L. C. Davis (private communication).
- ⁴⁰Y. Yafet, *Phys. Rev. B* **21**, 5023 (1980).
- ⁴¹In this, our method differs from the one employed in Refs. 6 and 7 for $\text{Cd}_{1-x}\text{Mn}_x\text{Te}$, where only "pure" CIS spectra from the ternary semiconductor were discussed.
- ⁴²CIS from different cleaves were normalized to each other using the integrated photoemission intensity of the Cd 4d core levels from each cleave, and the value of $(1-x)$ derived from the microprobe analysis.
- ⁴³In principle, other Auger and *sp*-related transitions may also contribute to the overall spectrum.
- ⁴⁴In Ref. 6, Ley *et al.* fitted experimental CIS spectra in terms of a Fano line shape with fixed E_0 and Γ (49.55 ± 0.05 eV and 0.85 eV, respectively, at all initial-state energies), and determined asymmetry parameters q generally around 2.45 and dropping to about 2.0 for initial-state energies within 2.2 eV of the valence-band maximum. Such values are partially consistent with those in Table I, which were, however, determined through a three-parameter least-squares-fitting procedure. The variations in E_0 , Γ , and q , that we report in Table I, even if present in $\text{Cd}_{1-x}\text{Mn}_x\text{Te}$, cannot be detected with the fitting procedure used in Ref. 6.
- ⁴⁵G. P. Williams, G. J. Lapeyre, J. Anderson, F. Cerrina, R. E. Dietz, and Y. Yafet, *Surf. Sci.* **89**, 606 (1979).
- ⁴⁶A. Franciosi and J. H. Weaver, *Phys. Rev. B* **27**, 3554 (1983).
- ⁴⁷A. Franciosi, J. H. Weaver, N. Martensson, and M. Croft, *Phys. Rev. B* **24**, 3651 (1981); M. Croft, A. Franciosi, J. H. Weaver, and A. Jayaraman, *ibid.* **24**, 544 (1981).